PERGAMON

International Journal of Heat and Mass Transfer 45 (2002) 4353–4359

International Journal of HEAT and MASS TRANSFER

www.elsevier.com/locate/ijhmt

Technical Note

Numerical simulation for heat and fluid characteristics of square duct with discrete rib turbulators

K. Tatsumi [a,*], H. Iwai [a], K. Inaoka [b]

[a] Department of Mechanical Engineering, Kyoto University, Sakyo-ku, Kyoto 606-8501, Japan

[b] Department of Mechanical and Systems Engineering, Doshisha University, Kyotanabe, Kyoto 610-0321, Japan

Received 15 March 2002; received in revised form 12 April 2002

1. Introduction

Attachment of rib turbulators to flow passages is one of the popular means of heat transfer enhancement. Typical use of the rib turbulators is found for example in the serpentine cooling air channel for the internal cooling of the gas turbine blades. Many studies therefore have been carried out for the heat transfer in ribbed channels and various types of ribs have been tested. A standard case of full-span ribs attached perpendicularly to the flow direction has been the first target and its friction and heat transfer characteristics have been reported in the references [1–3]. Further studies were made for other cases of attaching oblique ribs and V-shaped ribs to the channel wall. In these cases, secondary flow is incurred in the channel and enhances the fluid mixing between the near wall and core regions in the duct, eventually resulting in the enhancement of local heat transfer at the channel walls [4–6].

Discrete ribs also drew attention with which heat transfer enhancement due to the incurred secondary flow is achieved paying smaller pressure loss penalty [7–10]. In relation with the existence of the spanwise gaps, secondary flows are generated downstream their spanwise edges. Generation of the secondary flows in addition to the flow separation and reattachment makes the phenomenon quite complicated with the discrete ribs. Detailed studies of the flow structure and characteristics of the related heat transfer are required but such studies have scarcely been made so far.

In the present article, some results of the three-dimensional numerical computation conducted for flow and thermal fields over two types of array of ribs attached to a channel wall will be presented. One is of full-span ribs and the other is of discrete ribs, where both arrays are attached in a position perpendicular to the flow direction. The discussion will be given to the effects of three-dimensionality and unsteadiness of the flow and thermal fields for twofold purposes, one to test the applicability of numerical study to the type of flow under concern and another to provide hints to experimental works to be made in future.

2. Computational procedure

The governing equations solved in the present numerical study are the three-dimensional, incompressible, time dependent continuity, momentum and energy equations employing an eddy viscosity turbulence model. Attachment of discrete ribs to the channel and the high Reynolds number to be treated, as will be shortly shown, make the application of direct numerical simulation difficult. Therefore, RANS model approach has been chosen in the present study. Considering a possibility that significant magnitude of apparent shear stress is produced by the flow unsteadiness related to the periodical formation of vortices and regulates the flow pattern as is in a two-dimensional backward-facing step flow [11], unsteady flow computation was applied in the present study. Therefore, the equations to be solved are of the following forms:

$$\frac{D\rho}{Dt} = -\rho\left(\frac{\partial U_j}{\partial x_j}\right) \tag{1}$$

$$\frac{D\rho U_i}{Dt} = -\frac{\partial P}{\partial x_i} + \frac{\partial}{\partial x_j}\left(\mu\frac{\partial U_i}{\partial x_j} - \rho\overline{u_i' u_j'}\right) \tag{2}$$

* Corresponding author. Tel.: +81-75-753-5219; fax: +81-75-771-7286.

E-mail address: ktatsumi@mbd.nifty.com (K. Tatsumi).

0017-9310/02/$ - see front matter
PII: S0017-9310(02)00141-2

Nomenclature

AR	duct aspect ratio
C_f	skin friction coefficient
D	hydraulic diameter
e	rib height
H	duct height
k	turbulence kinetic energy
Nu	Nusselt number based on D and bulk mean temperature
Nu_0	Nusselt number for a smooth tube
p	rib pitch
P	local mean pressure
Pr	Prandtl number
Pr_t	turbulent Prandtl number
Re	Reynolds number
Sc	Schmidt number
Sc_t	turbulent Schmidt number
Sh	Sherwood number based on D and bulk mean concentration
Sh_0	Sherwood number for a smooth tube
u', v', w'	fluctuating velocity components
U, V, W	mean velocity components
w_r	rib stream chord length
W_D	duct width
W_{G1},W_{G2}	gap width for discrete ribs
x, y, z	spatial coordinate system
Y', Y	fluctuating and mean mass fractions

Greek symbols

$\tilde{\varepsilon}$	isotropic dissipation rate
θ', Θ	fluctuating and mean temperatures
ρ	density
μ	viscosity
ν_t	turbulent kinetic viscosity

$$\frac{D\rho\Theta}{Dt} = \frac{\partial}{\partial x_j}\left(\frac{\mu}{Pr}\frac{\partial\Theta}{\partial x_j} - \rho\overline{u_j'\theta'}\right) \tag{3}$$

As for the turbulence model to be applied for the Reynolds shear stress in Eq. (2), a non-linear eddy viscosity model proposed by Craft, Launder and Suga (hereafter referred to CLS model) [12] has been adopted. As has been discussed above, flow around a discrete rib is of highly three-dimensional nature. In the reference [13] for a backward-facing step flow, several turbulence models were tested. CLS model was observed best in capturing the three-dimensional vortical structure in a separating and reattaching flow region. On the other hand, the following gradient type of eddy viscosity model is adopted for the turbulent heat flux:

$$-\overline{u_j'\theta'} = \frac{\nu_t}{Pr_t}\frac{\partial\Theta}{\partial x_j} \tag{4}$$

where turbulent Prandtl number, Pr_t was assumed to be constant and equal to 0.9. For the purpose to compare with the mass transfer experiments of Cho and coworkers [8,9] using naphthalene sublimation technique, mass transfer equation was also solved. Mass conservation equation for naphthalene to be solved is:

$$\frac{D\rho Y}{Dt} = \frac{\partial}{\partial x_j}\left(\frac{\mu}{Sc}\frac{\partial Y}{\partial x_j} - \rho\overline{u_j'Y'}\right) \tag{5}$$

where Y is the mass fraction of naphthalene, and Sc is the Schmidt number for binary diffusion of naphthalene into air. As for the turbulent mass flux, gradient type of closure model similar to Eq. (4) is adopted by replacing the turbulent Prandtl number by the turbulent Schmidt number, Sc_t. Value of Sc_t was set equal to 0.9.

To solve the dynamical fully developed flow and thermal fields of a rib-roughened channel, periodical boundary conditions were applied to the streamwise boundaries. To modulate the linear pressure decay in the streamwise direction of the periodical unit, the procedure proposed by Patankar et al. [14] was adopted in solving Eq. (2). By modifying the constant of this modulated term of pressure, the objective mass flow rate, namely the Reynolds number, was attained. As for solving the temperature and concentration fields, two different methods were employed. For the temperature field having constant heat flux conditions at walls, the same process indicated in the reference [14] was applied, i.e. a modulated term is added to Eq. (3). For the concentration field, since a constant concentration condition is applied at the walls, a boundary condition having the non-dimensional value of $(Y - Y_w)/(Y_b - Y_w)$ equal at the inlet and outlet boundaries was employed. Here, Y_w and Y_b are the wall mass fraction and the bulk mean mass fraction, respectively, where Y_b at the inlet was fixed at a constant value.

Fully implicit forms of finite-difference equivalents of the governing equations were solved numerically along the time axis in a manner adopted in the reference [15]. High order difference scheme was applied for finite-differencing the momentum equations in that study. In the energy equation, species mass conservation equation and the two governing equations for k and $\tilde{\varepsilon}$, a first-order upwind scheme was adopted for the convection

terms and a central-difference scheme for the diffusion terms. Pressure gradient in the momentum equation was evaluated by solving the pressure correction with the SIMPLE algorithm so as to satisfy the finite difference equivalent of Eq. (1). Alternating direction implicit method was employed for iterative procedure needed to solve those of elliptic-type partial differential equations.

3. Results and discussion

3.1. Full-span ribs

Fig. 1(a) illustrates the geometry of the flow space and the computational domain adopted in the present study for the full-span ribs with 90° inclination against the flow direction. Ribs are attached to the top and bottom wall surfaces in a symmetric pattern with respect to the horizontal mid-plane of the channel. Channel aspect ratio is $AR = 1$ so that hydraulic diameter of the channel is $D = H$ where H is the channel height. Rib height to duct height ratio (e/H), rib height to rib stream chord length ratio (e/w_r) and rib streamwise pitch to rib height ratio (p/e) are set as $e/H = 0.08$, $e/w_r = 0.8$ and $p/e = 8$, respectively. Flow Reynolds number based on the channel hydraulic diameter is chosen to be $Re =$ 30,000. All these conditions match the counterparts of the naphthalene sublimation experiments reported by Cho et al. in the reference [9]. For comparison with their experimental data, therefore, species mass conservation equation of naphthalene was solved in place of energy equation setting the Schmidt number equal to 2.25. Constant concentration is assumed at the duct top and bottom walls as the boundary condition. At the duct sidewalls and rib surface, zero normal gradient of naphthalene concentration is assumed.

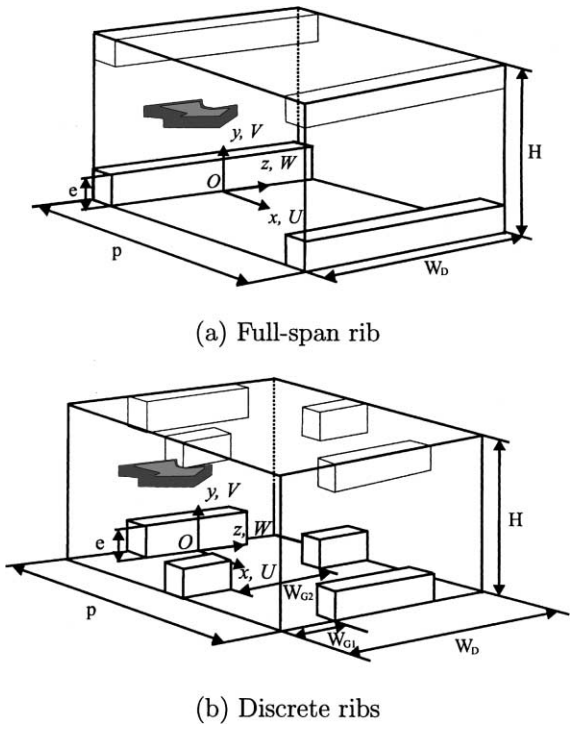

Fig. 1. Computational domains.

Before moving on to the detail discussions, it should be noted that periodical fluctuations of flow were observed in the streamwise and spanwise directions. However, due to the small aspect ratio of the duct and to low height of the rib, the fluctuation intensity appeared to be small. Therefore, in the present article, time mean results are only shown and the effect of the apparent shear stress will not be discussed here.

Fig. 2(a) compares the computed streamwise distribution of Sh/Sh_0 along the centerline of the channel bottom wall with the experimental data obtained by Cho et al. [9]. Here Sh_0 is the following McAdams equation for the fully developed turbulent flow in a circular tube [16]:

$$Sh_0 = 0.023Re^{0.8}Pr^{0.4}(Sc/Pr)^{0.4} \tag{6}$$

First of all, computed results are observed to agree fairly well with the experimental data. Therefore, the numerical scheme adopted in the present study is validated in this point. Reason for the discrepancy found in the present results from the experimental data is briefly discussed here. As is well known, flow recirculation region exists downstream the rib. In some parts of the recirculation region, Sh/Sh_0 is expected to take a value smaller than unity but is actually larger than unity. So, experimental data should have some inaccuracy in this sense. Additionally, constant concentration assumption taken as the boundary condition must be revisited. Sublimation is a phenomenon to be categorized as simultaneous heat and mass transfer. Therefore, its rate is regulated by the supplying rate of the latent heat or by the convection heat transfer from the fluid and by the heat conduction through naphthalene cast layer. For smooth surfaces, non-uniformity is insignificant in the distribution of heat transfer rate so that uniformity of the naphthalene concentration at the surface or of the surface temperature is a good approximation of the real phenomenon. However, this may not be the case of the present ribbed surface. These points must be studied in detail in future experimental and numerical studies.

Fig. 2(b) displays the spatial distribution of Sh/Sh_0. Sherwood number takes high value around the flow reattachment point $x/e \simeq 4.2$ over a wide central part of the channel. Sh/Sh_0 is small in the first half of the flow recirculation region except for a small region adjacent the back surface of the rib and takes highest value at $6.5 \leqslant x/e \leqslant 6.75$ just in front of the rib. Spanwise

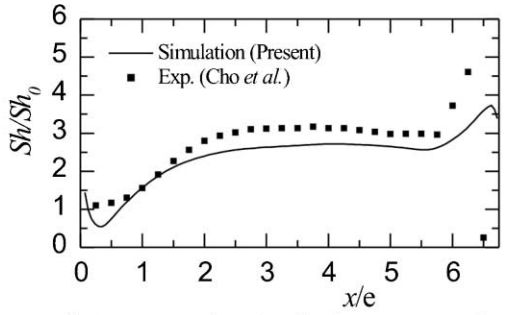

(a) Sh/Sh_0 streamwise distribution at centerline

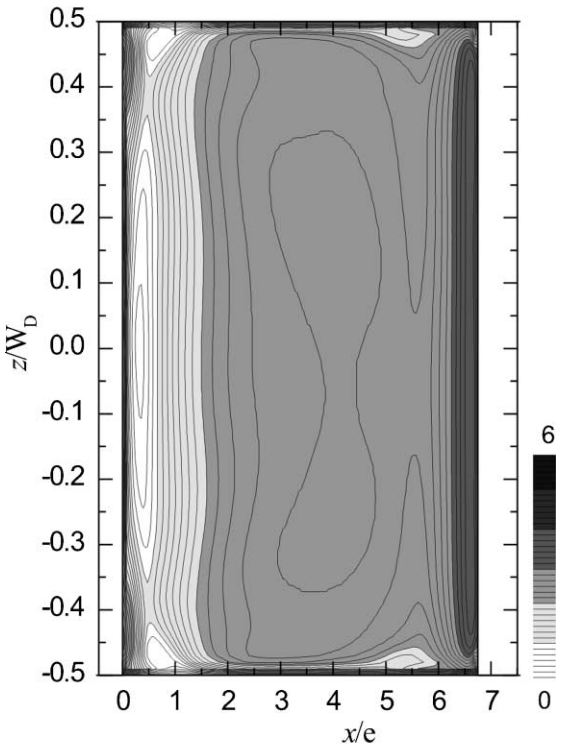

(b) Sh/Sh_0 contour distribution

Fig. 2. Sherwood number distributions.

non-uniformity of Sh/Sh_0 reflects the three-dimensionality of the flow.

3.2. Discrete ribs array

Computational domain for the channel attached with an array of the discrete ribs is illustrated in Fig. 1(b). As is seen, two types of discrete ribs, one rib having gaps from the sidewalls at both ends (hereafter called DR-1 rib) and another having interruption in the center (hereafter called DR-2 rib), are attached alternately at a periodical pitch. The illustrated array of the discrete ribs is

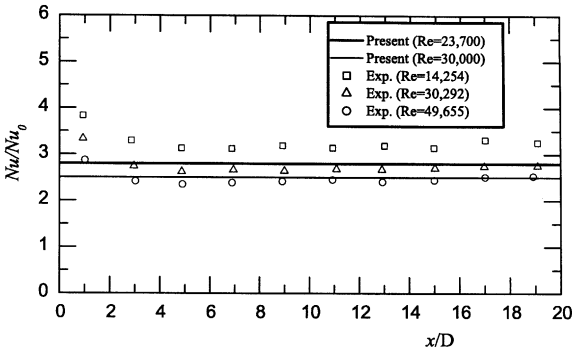

Fig. 3. Averaged Nusselt number.

attached to both of the top and bottom wall surfaces in an in-phase fashion. Geometry of the ribs is set to match the experiments done by Han and Zhang [7]. Streamwise pitch of the array is $p/e = 10$ and rib height to duct height ratio is $e/D = 0.0625$. The duct aspect ratio is unity, i.e. $AR = 1$, as was in the full-span rib case. The gap width to duct width ratio is same both for DR-1 rib and DR-2 rib, i.e. $W_{G1}/W_D = W_{G2}/W_D = 0.33$. Reynolds number based on the hydraulic diameter of the channel is changed in two steps, i.e. $Re = 23{,}700$ and $Re = 30{,}000$. Constant heat flux is assumed as the thermal condition in the present computation at all surfaces including the sidewalls and the rib surfaces.

Fig. 3 shows the comparison between the presently computed results and the experiments done by Han and Zhang [7]. In the figure are shown the streamwise change of the local spatial mean of the Nusselt number, i.e. a value obtained by averaging the local Nusselt number over each streamwise pitch of the array at the rib-roughened surfaces. Results are plotted in a normalized form and Nu_0 is the following counterpart of a fully developed turbulent flow in a circular tube as in the above discussion for the full-span ribs:

$$Nu_0 = 0.023 Re^{0.8} Pr^{0.4} \tag{7}$$

Since the present computation was done for a single pitch of the array assuming dynamical fully-developed state of the flow and thermal fields, computed value is shown as a horizontal line over the whole streamwise positions studied in the experiments. The presently computed results show good agreement with the experimental data reported by Han and Zhang. Therefore, the present numerical method can be used as a tool to predict the thermal performance of ribbed heat transfer surfaces. For further information, the obtained numerical results for the case of $Re = 30{,}000$ are now discussed in detail in the following.

Spatial distribution of the local Nusselt number is plotted in Fig. 4(a). Comparing this figure with Fig. 2(b), discrete ribs are judged to be more effective in the en-

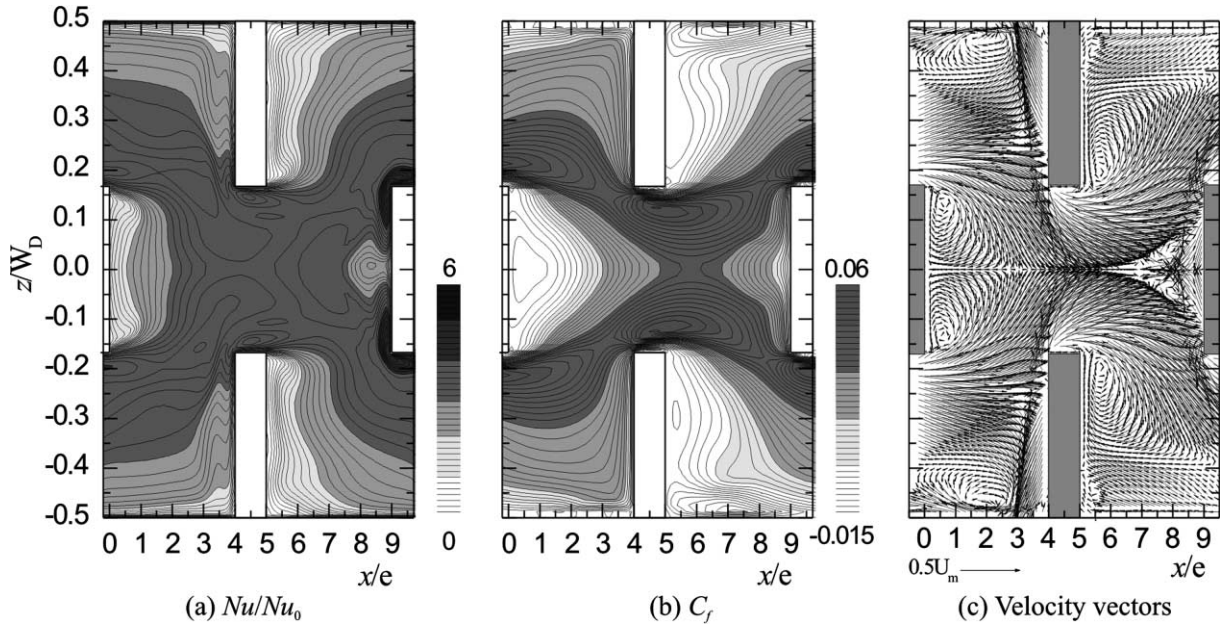

Fig. 4. Distributions at and near duct bottom wall surface ($Re = 30{,}000$).

hancement of wall heat transfer. The region where Nu/Nu_0 takes a value larger than 3 is noticeably wider in area with the discrete ribs than with the full-span ribs. Fig. 4(b) shows the spatial distribution of skin friction coefficient, C_f, on the bottom wall surface. White parts in the figure correspond to the region where C_f takes negative value or where back flow appears near the bottom wall. Nu/Nu_0 takes large value in the gaps besides the rib where C_f takes large positive value too. This indicates that the flow going by the rib in the gap keeps the heat transfer coefficient high there. In addition to this, white part behind the DR-1 rib is of triangular shape and is contracted in area in comparison with the counterpart of the full-span rib. These are the main reasons of the effectiveness of the studied discrete ribs in heat transfer enhancement. Fig. 5 shows the velocity vector maps for secondary flow in the cross sections at four streamwise positions $x/e = 0.0$, 2.0, 5.0 and 7.0, and the fluid temperature contours in the same cross sections. At $x/e = 0.0$, downwash flow appears in the inner half of the gaps near the center rib and assists the large scale fluid mixing. So low fluid temperature isotherms (white area in figure) approach the bottom wall there and Nu/Nu_0 takes values larger than 3. This kind of highly three-dimensional flow and therefore the protrusion of low fluid temperature region toward the bottom wall are observed at other three positions as well and produce the expansion of the area of high Nusselt number region. One more noticeable point in the figure is that a pair of counter-rotating streamwise vortices persistently exists near the sidewalls of the channel. These vortices are effective to enhance the heat transfer from the sidewalls, although the sidewall heat transfer is not the point to be discussed in the present study.

These large scale secondary flows accompanying the downwash flow are not generated in the case of full-span ribs. One more thing to be discussed is the tornado type vortices. Fig. 4(c) displays the velocity vector maps in an x–z plane at $y/e = 0.1$. Generation of tornado type vortices is clearly depicted behind each rib. Since flow goes around the rib in the gap with high velocity and more intense shear layer is produced besides the rib edge, these vortices become more intense and larger in scale in the discrete rib case than in the full-span rib case. Although tornado vortices incur the heat transfer deterioration at positions inside the vortices, they are effective in reducing the streamwise flow recirculation region or in making the recirculation region in a triangular shape as is pointed out in Fig. 4(b). Therefore, the tornado vortices are also expected to be effective in enhancing the wall heat transfer.

4. Concluding remarks

Three-dimensional unsteady flow computation was carried out with RANS approach employing the CLS model in the present study for flows in a square duct having roughened walls with an array of full-span ribs or with another array of discrete ribs. The predicted streamwise distribution of Nusselt number is in good agreement with the experimental data for both arrays.

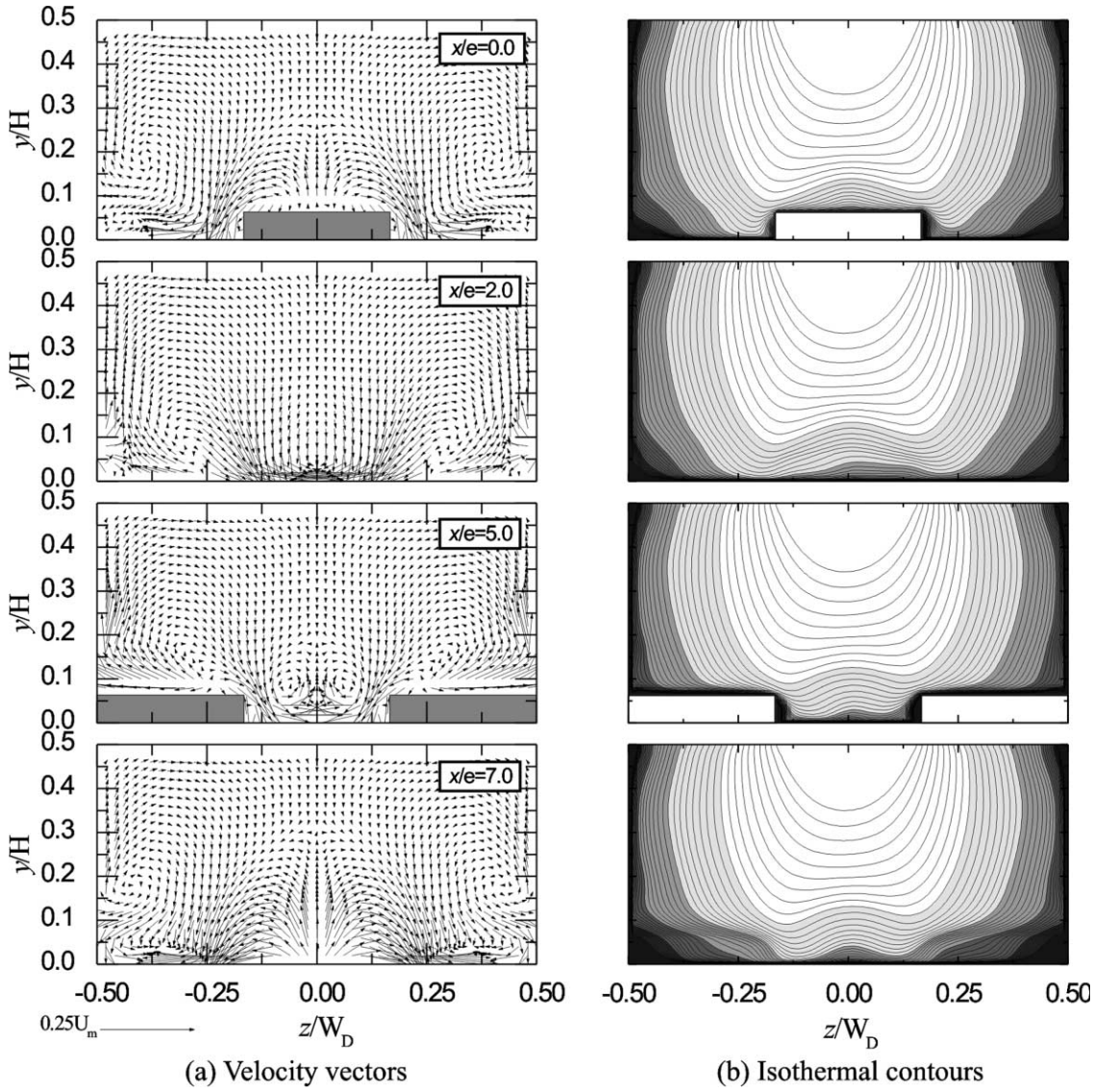

Fig. 5. Velocity vectors and isothermal contours ($Re = 30{,}000$).

Flow generated in the duct and its related heat transfer is highly three-dimensional even in the case with full-span ribs when their rib height to duct height ratio is small. For the discrete rib case, flows going by the rib accompany a pair of counter-rotating large scale streamwise vortices and enhance the flow mixing. This keeps the wall heat transfer higher. Tornado type transverse vortices appearing behind the edge of the rib become more intense and larger in scale in the duct roughened with discrete ribs. Generation of this type of vortices is effective to reduce the area of the flow recirculation region and is effective to enhance the wall heat transfer.

These pictures suggested for the flows in the duct having rib-roughened walls give clues for future comprehensive experimental works.

References

[1] J.C. Han, Heat transfer and friction characteristics in rectangular channels with rib turbulators, ASME J. Heat Transfer 110 (1988) 321–328.
[2] T.-M. Liou, J.-J. Hwang, S.-H. Chen, Simulation and measurement of enhanced turbulent heat transfer in a

channel with periodic ribs on one principal wall, Int. J. Heat Mass Transfer 36 (2) (1993) 507–517.
[3] G. Rau, M. Cakan, D. Moeller, T. Arts, The effect of periodic ribs on the local aerodynamic and heat transfer performance of a straight cooling channel, ASME J. Turbomach. 120 (1998) 368–375.
[4] J.C. Han, J.S. Park, Developing heat transfer in rectangular channels with rib turbulators, Int. J. Heat Mass Transfer 31 (1) (1988) 183–194.
[5] M.E. Taslim, T. Li, D.M. Kercher, Experimental heat transfer and friction in channels roughened with angled v-shaped and discrete ribs on two opposite walls, ASME J. Turbomach. 118 (1996) 20–28.
[6] R. Kiml, S. Mochizuki, A. Murata, Effects of rib arrangements on heat transfer and flow behavior in a rectangular rib-roughened passage, ASME J. Heat Transfer 123 (2001) 675–681.
[7] J.C. Han, Y.M. Zhang, High performance heat transfer ducts with parallel broken and v-shaped broken ribs, J. Heat Mass Transfer 35 (2) (1992) 513–523.
[8] H.H. Cho, S.J. Wu, H.J. Kwon, Local heat/mass transfer measurements in a rectangular duct with discrete ribs, ASME J. Turbomach. 122 (2000) 579–586.
[9] H.H. Cho, S.Y. Lee, S.J. Wu, The Combined Effects of Rib Arrangements and Discrete Ribs on Local Heat/Mass Transfer in a Square Duct, An ASME paper, 2001-GT-175, 2001.
[10] K. Inaoka, D. Yamashita, H. Tani, M. Senda, Flow visualization and heat transfer measurements of a duct flow with full-span and interrupted rib turbulators, in: Proceedings of the 3rd International Symposium on Advanced Energy Conversion Systems and Related Technologies, Nagoya, 2001, pp. 395–400.
[11] K. Tatsumi, K. Iwai, K. Inaoka, K. Suzuki, Prediction of time-mean characteristics and periodical fluctuation of velocity and thermal fields of backward-facing step, in: Proceedings of the 1st International Symposium on Turbulence and Shear Flow Phenomena, Santa Barbara, CA, 1999, pp. 1167–1172.
[12] T.J. Craft, B.E. Launder, K. Suga, Development and application of a cubic eddy-viscosity model of turbulence, Int. J. Heat Fluid Flow 17 (1996) 108–115.
[13] H. Iwai, E.C. Neo, K. Suzuki, Numerical study on three-dimensional flow and heat transfer characteristics of turbulent flows over a backward-facing step in a rectangular duct, in: Proceedings of the Symposium on Energy Engineering in the 21st Century, Hong Kong, 2000, pp. 161–168.
[14] S.V. Patankar, C.H. Liu, E.M. Sparrow, Fully developed flow and heat transfer in ducts having streamwise-periodic variations of cross-sectional area, ASME J. Heat Transfer 99 (1977) 180–186.
[15] H. Iwai, K. Nakabe, K. Suzuki, Flow and heat transfer characteristics of backward-facing step laminar flow in a rectangular duct, Int. J. Heat Mass Transfer 43 (3) (2000) 457–471.
[16] W.H. McAdams, Heat Transmission, second ed., McGraw-Hill, New York, 1942.